Design of a Predictive Current Controller for a Separated Starter-Generator Application

J.Hobraiche[1 2] J.P. Vilain[1] F.X. Bernard[2]
[1] University of Technology of Compiègne
Laboratory of Electromechanics / BP20529
60205 Compiègne Cedex / France
Tel.: +33 / (0) – 344.23.45.07
Fax: +33 / (0) – 344.23.79.37
E-Mail: Julien.Hobraiche@utc.fr
E-Mail: Jean-Paul.Vilain@utc.fr
URL: http://www.utc.fr/lec

[2] Valeo Electrical System
2, rue A. Boulle / BP 150
94017 Créteil Cedex / France
Tel.: +33 / (0) – 148.98.85.71
Fax: +33 / (0) – 142.07.29.82
E-Mail: Francois-Xavier.Bernard@valeo.com
URL: http://www.valeo.com

Keywords

Pulse Width Modulation (PWM), Automotive Application, Converter Control

Abstract

This paper proposes a predictive current controller to control the phase currents of a separated starter-generator (SSG) on the whole speed range. A comparison with hysteretic current controller and regulation in d-q axis is done to highlight the spectral benefits of predictive controller at high speed.

Introduction

Since the last two decades, the electrical power requirement in an automobile has been linearly increasing because of new added functions [1]. Moreover, decrease of fuel consumption and reduction of emissions of carbon dioxide have obliged car manufacturers and automotive suppliers to study opportunities of a starter-generator application [2]. Here a smooth synchronous wound rotor machine with eight pole pairs driven by a belt with a 3:1 ratio is studied. A three-phased inverter working in PWM mode is used to supply the SSG. The switching frequency of each leg of the inverter is limited at 20 kHz.
The fundamental frequency of the phase current can reach 2400 Hz. Moreover, phase currents can be up to 800 Â in starter mode (transient) and 550 Â in alternator/boost mode (steady state operation). High losses in the inverter can occur and reduction of power losses in the inverter has to be considered [3].
Firstly, mathematical models of the SSG and inverter are described. Benefits and drawbacks of the d-q axis controller followed by a Space Vector Modulation (SVM) [4] and the hysteretic current controller [5] are pointed out. Then a proposition for a predictive current controller is developed. Simulation results show the advantages of such controller. Experimental test bench and hardware are also presented.

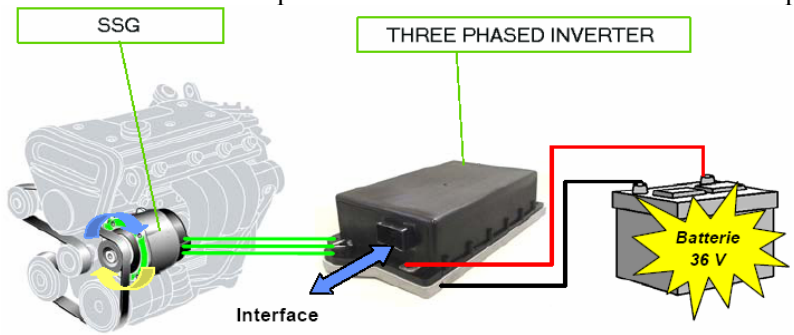

Fig. 1 : Separated starter-generator

SSG Modeling

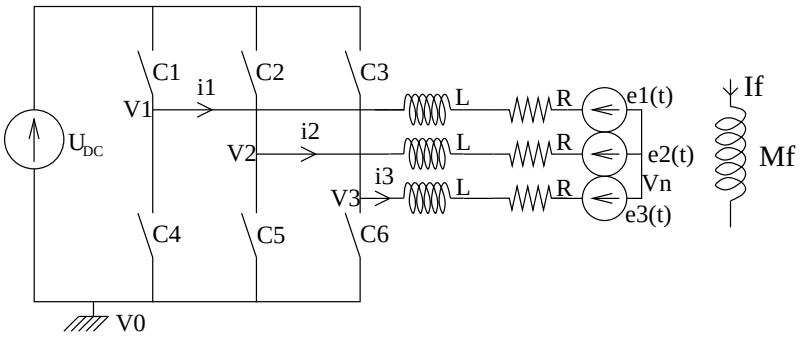

Fig. 2 : Topology

The equivalent electronic schematic is described on Fig.2. The DC-link voltage comes from a classical battery. It is supposed ideal and modelled by a simple constant DC-voltage U_{DC}. The inverter is composed by six switches C_1 to C_6. In order not to short circuit the battery, a dead time is respected between C_i and C_{i+3}. We define the switching function SC_i of the switches C_i by:

$$SC_i = \begin{cases} +1 & if\ C_i\ is\ on \\ -1 & if\ C_i\ is\ off \end{cases} \quad (1)$$

The vectorial approach of the inverter defines the output vector of the inverter by:

$$\bar{V} = \frac{2}{3}\left(SC_1 + a.SC_2 + a^2.SC_3\right).\frac{U_{DC}}{2} \text{ where } a = e^{j\frac{2.\pi}{3}} \quad (2)$$

There are eight possibilities for the output vector sum up in the Tab. 1 and plotted in the stator reference frame on Fig. 3.

Table I : Output voltage vector of the three phased inverter

Output Vector	SC_1	SC_2	SC_3
$\bar{V}_0$	-1	-1	-1
$\bar{V}_1$	+1	-1	-1
$\bar{V}_2$	+1	+1	-1
$\bar{V}_3$	-1	+1	-1
$\bar{V}_4$	-1	+1	+1
$\bar{V}_5$	-1	-1	+1
$\bar{V}_6$	+1	-1	+1
$\bar{V}_7$	+1	+1	+1

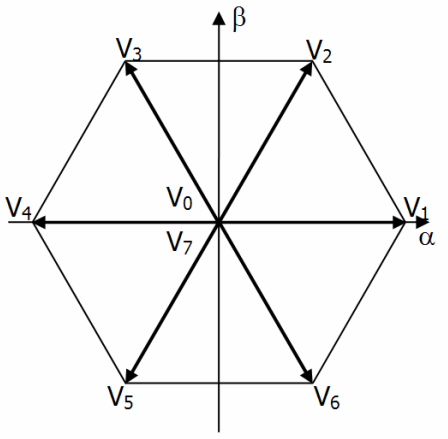

Fig. 3 : Output voltage vector

The following equation of the wound rotor synchronous machine in the stator reference frame is assumed:

$$\bar{V} = \bar{E} + R.\bar{I} + L\frac{d\bar{I}}{dt} \quad (3)$$

$\bar{E}$ is the back emf voltage vector. It turns at the electrical pulsation ω_s and has a norm $\left|\bar{E}\right| = \sqrt{2/3}M_f.I_f.\omega_s$. The purpose of the current controller is to define the switching functions SC_i in order to generate a current vector $\bar{I}$ as close as possible to the current reference vector $\bar{I}^*$.

Classical Current Controllers

In order to strictly follow the current reference $\bar{I}^*$, two well-known strategies were primarily tested. The first one is the classical regulation in d-q axis modified with a SVM technique. The second one is the hysteretic current control.

Regulation in d-q axis

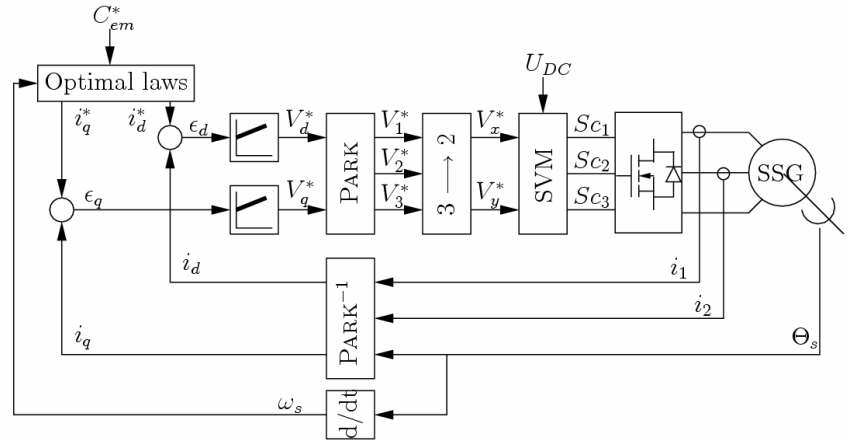

Fig. 4 : Regulation in d-q axis synoptic

The synoptic of the regulation in d-q axis is plotted on Fig. 4.Optimal control laws of the SSG determine the reference current i_d^* and i_q^* in function of the torque reference C_{em}^* and electrical pulsation ω_s. By sensing two of the three phase currents and the position, the real current i_d and i_q are determined thanks to an inverse Park transformation. Then the two error signals ε_d and ε_q are corrected by proportional plus integral correctors. Outputs of the two correctors are the reference voltage vector in d-q reference frame. After a Park transformation, the three phase voltage reference V_1^*, V_2^* and V_3^* are calculated. Classically, these references are compared with a triangular carrier so as to determine the switching function $SC_i(t)$ of leg i. With this method the maximum modulus of the voltage reference vector in steady-state without overmodulation is $\hat{V}_i = U_{DC}/2$. As far as our machine is an isolated three wires one, we can add a zero sequence signal to each reference voltage so as to increase the maximum linearity of the inverter to $\hat{V}_i = 2/\sqrt{3} \times U_{DC}/2 \approx 1.15 \times U_{DC}/2$. A classical way to do it is to use a SVM technique [6-7].

To evaluate the spectral characteristics of the different strategy, a vectorial spectrum is calculated. It represents the quality of the PWM by calculating the direct and inverse rotating vector induced by spectral harmonic of the three differential voltage $V_{12}=V_1-V_2$, $V_{13}=V_1-V_3$ and $V_{23}=V_2-V_3$ [8]. A voltage vector can be decomposed in direct rotating vector and indirect rotating vector:

$$\overline{V(t)} = \overline{V_1}.e^{j\omega_s t} + \sum_{n=2}^{\infty} \left(\underbrace{\overline{V_{n+}}.e^{j\omega_s t}}_{\text{direct rotating vector}} + \underbrace{\overline{V_{n-}}.e^{-j\omega_s t}}_{\text{indirect rotating vector}} \right) \quad (4)$$

With SVM technique the switching frequency of the inverter is constant. In steady-state, the vectorial spectrum of the voltage vector is composed by a fundamental component and harmonics at sidebands of the switching frequency and its multiples. Simulation results for an alternator point are plotted on Fig. 5. If the fundamental frequency increases, the fundamental component and the sidebands of the switching frequency become closer and closer. As a result, operation in PWM mode is not possible at frequencies upper than 1000 Hz because the corrector tries to compensate the phase currents distortion which is produced in the loop itself because of the low value of the frequency ratio $R=f_{PWM}/f_0$. For fundamental frequencies upper to 1000 Hz, a full-wave modulation is used in order to control the machine. The magnitude of the fundamental of the voltage vector is constant equal to $\hat{V}_i = 4/\pi \times U_{DC}/2$.

The only parameter is then the internal angle between the fundamental of the voltage vector and the back emf vector $\overline{E}$. To this major drawback can be added the classical phase error and magnitude error inherent to this regulation.

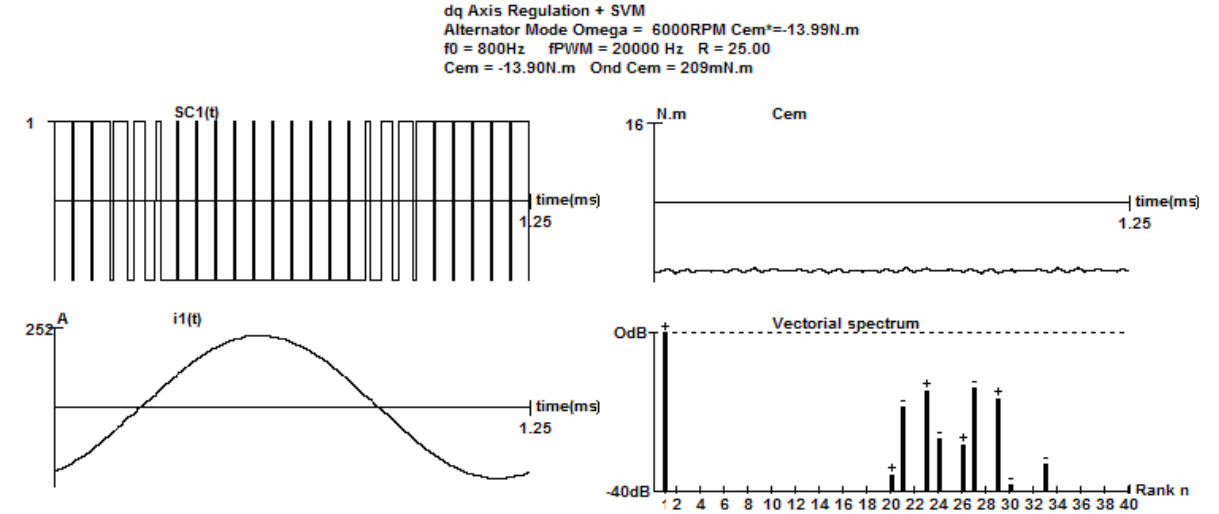

Fig. 5 : Simulation in alternator mode under d-q regulation with SVM

Hysteretic current controller

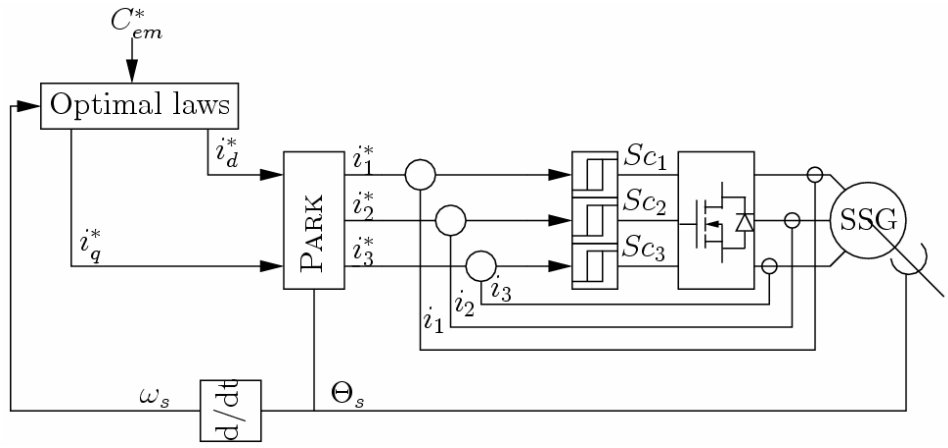

Fig. 6 : Hysteretic current controller synoptic

The operation mode of a hysteretic current controller is basic (Cf. Fig. 6~7) [9]. Each one of the phase currents follows the reference current thanks to the simple report that a phase current increases under positive voltage and decrease under negative voltage. The purpose of the hysteretic controller is to maintain the real current within an interval around the reference current. The only thing to define is the half width of the hysteretic window Δh (in A). The reference current of leg i is $i_i^*(t)$ and the real current is $i_i(t)$. The scalar error $\varepsilon_i(t) = i_i^*(t) - i_i(t)$ is computed. If the error is higher (Resp. lower) than Δh then $Sc_1(t) = +1$ (Resp. $Sc_1(t) = -1$). This kind of current controller is easy to implement, robust against parameter variations and highly dynamic. As far as the phase currents sum is null ($i_1 + i_2 + i_3 = 0$), there is an evident redundancy in the control which can lead to current error increase of two times Δh. For low reference modulation index $m_i^* = |V^*|/(U_{DC}/2)$, the density of harmonics is high in the vectorial spectrum [10] of voltage vector in spite of the high switching frequency.

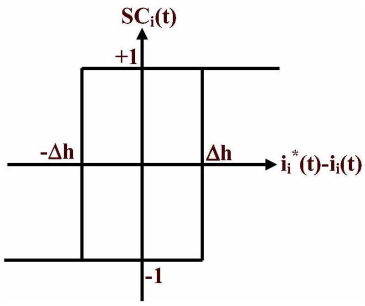

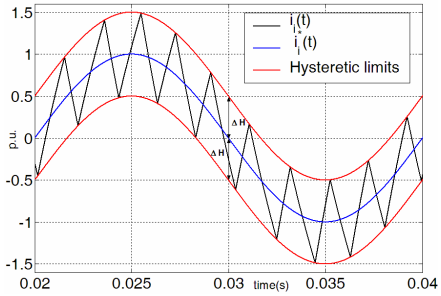

Fig. 7 : Hysteretic current controller principle

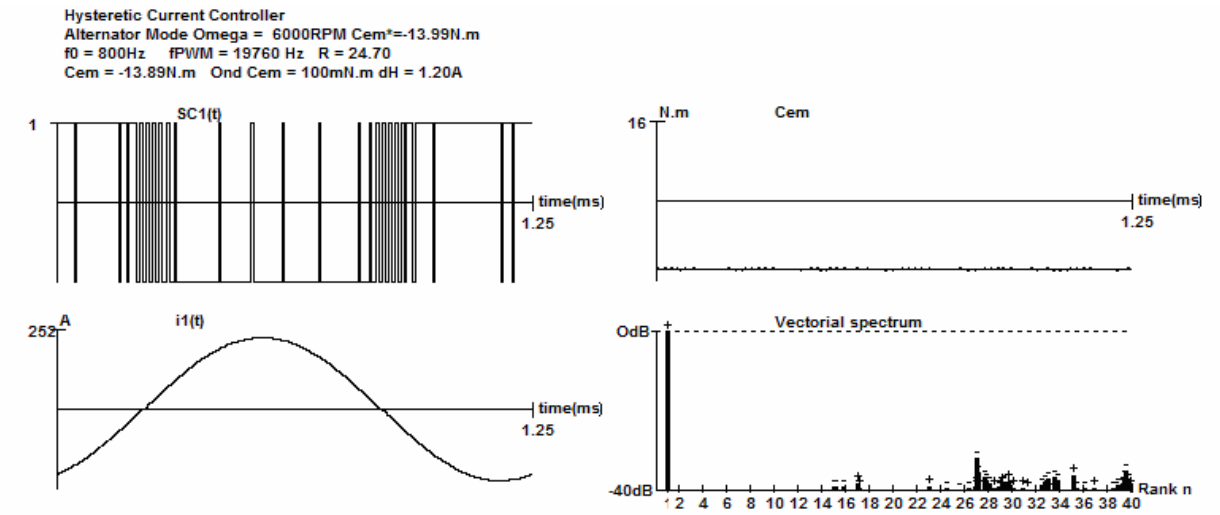

Fig. 8 : Simulation in alternator mode under hysteretic current control

As the regulation in d-q axis is not possible on the whole speed range of the SSG application and the hysteretic current controller is not optimal, a predictive current controller is designed in the next paragraph to determine optimal sequence of the three phase inverter. The approach developed by Holtz and Stadfeld [11][12] is retained and adapted to our case.

Design of the Predictive Current Controller

Preliminary calculations

The purpose of the predictive current controller is to maintain the modulus of the vectorial current error $\overline{\Delta I} = \bar{I} - \bar{I}^*$ under a certain value δI. In the stator reference frame, it means that $\overline{\Delta I}$ must strictly stay inside a circle of radius δI. Firstly, we have to predict the evolution of the current vector $\bar{I}$ by solving the following equation:

$$\tau_s \frac{d\bar{I}}{dt} + \bar{I} = \frac{1}{R}\left(\bar{V} - \bar{E}\right) \text{ where } \tau_s = \frac{L}{R} \tag{5}$$

We consider that the back emf vector turns uniformly with a constant modulus and the current vector is known (initial condition) at time $t=t_n$:

$$\begin{cases} \overline{E(t)} = E(t_n).e^{j.(\omega_s(t-t_n)+\varphi_n)} \\ \overline{I(t=t_n)} = \overline{I(t_n)} \end{cases} \tag{6}$$

If the reference vector $\bar{I}^*$ also turns uniformly with a constant modulus and is known at time t=t_n, the evolution of the vectorial current error can then be determined. As the switching frequency is high, we can approximate this evolution:

$$\overline{\Delta I_x}(t) = \overline{\Delta I_x}(t_n) + (t-t_n).\left[\underbrace{-i_x(t_n)/\tau_s + V_x/L - E(t_n)/(Z.\tau_s).\cos(\varphi_n - \psi) + E(t_n).\omega_s/Z.\sin(\varphi_n - \psi) + \omega_s.i^*{}_y(t_n)}_{a}\right]$$

$$\overline{\Delta I_y}(t) = \overline{\Delta I_y}(t_n) + (t-t_n).\left[\underbrace{-i_y(t_n)/\tau_s + V_y/L - E(t_n)/(Z.\tau_s).\sin(\varphi_n - \psi) - E(t_n).\omega_s/Z.\cos(\varphi_n - \psi) - \omega_s.i^*{}_x(t_n)}_{b}\right] \quad (7)$$

where $Z = \sqrt{R^2 + (L.\omega_s)^2}$ and $\psi = \tan^{-1}(L.\omega_s/R)$. With these results, the future evolution of the vectorial current error can be computed. The vectorial current error modulus is monitored. As soon as an output of the reference circle is detected, a new voltage vector has to be chosen between those of Tab. 1.

To choose between the seven vectors (the two freewheeling vectors $\overline{V_0}$ and $\overline{V_7}$ imply the same variation of $\overline{\Delta I}$) which one is the optimal, we first have to determine those which bring back the current vectorial error in the circle. On Fig. 9(a), two important angle are defined, the tangency angle δ_0 and the incidence angle δ of a possible trajectory for the vectorial current error. If at time t=t_n, the current vectorial error $\overline{\Delta I(t_n)}$ is outside of the reference circle, the tangency angle δ_0 and the incidence angle δ, for each candidate vector $\overline{V_i}$, can be calculated with the following equations:

$$\delta_0 = \sin^{-1}\left(\delta I / \left|\overline{\Delta I(t_n)}\right|\right) \text{ and } \delta = \cos^{-1}\left(\left(a.\Delta I_x(t_n) + b.\Delta I_y(t_n)\right) / \left(\left|\overline{u}\right|.\left|\overline{\Delta I(t_n)}\right|\right)\right) \quad (8)$$

If the incidence angle δ is greater than the tangency angle δ_0 then the voltage vector $\overline{V_i}$ brings back the current vectorial error in the reference circle. There can be several vectors with an incidence angle $\delta > \delta_0$. To decide between voltage vectors which bring back the current vectorial error in the circle, the predicted time to the next output of current vectorial error is computed. The chosen vector is the one that delay the most the next predicted output of the current vectorial error in order to decrease the switching frequency for a given radius δI. To calculate the intersection between the approximate straight line trajectory and the reference circle, the following equation is solved:

$$\left|\overline{\Delta I(t_n + \Delta t)}\right|^2 = \delta I^2 \quad (9)$$

It is a second degree equation. The solutions are:

$$D_{is} = \left(a.\Delta I_x(t_n) + b.\Delta I_y(t_n)\right)^2 - \left(a^2 + b^2\right)\left(\Delta I_x{}^2(t_n) + \Delta I_y{}^2(t_n) - \delta I^2\right)$$

$$\Delta t = \frac{-\left(a.\Delta I_x(t_n) + b.\Delta I_y(t_n)\right) \pm \sqrt{D_{is}}}{a^2 + b^2} \quad (10)$$

If $\delta > \delta_0$ then $D_{is} > 0$ and the equation admits two solutions. The first solution $\Delta t_1 = (-\left(a.\Delta I_x(t_n) + b.\Delta I_y(t_n)\right) - \sqrt{D_{is}})/(a^2 + b^2)$ represents the interval of time between t_n and the date of entry in the reference circle. The second solution $\Delta t_2 = (-\left(a.\Delta I_x(t_n) + b.\Delta I_y(t_n)\right) + \sqrt{D_{is}})/(a^2 + b^2)$ is the interval of time between t_n and the date of exit of the circle (See Fig. 11(b)). The optimal vector with an incidence angle $\delta > \delta_0$ is the one which maximises the interval of time Δt_2.

If none of the vectors have an incidence angle $\delta > \delta_0$, the vector which minimizes the distance between center of the reference circle and the affix of $\overline{\Delta I(t_n + \Delta t_{\min})}$ is chosen. $\Delta t_{\min}$ represents the minimum pulse width allowable by a switch of the inverter.

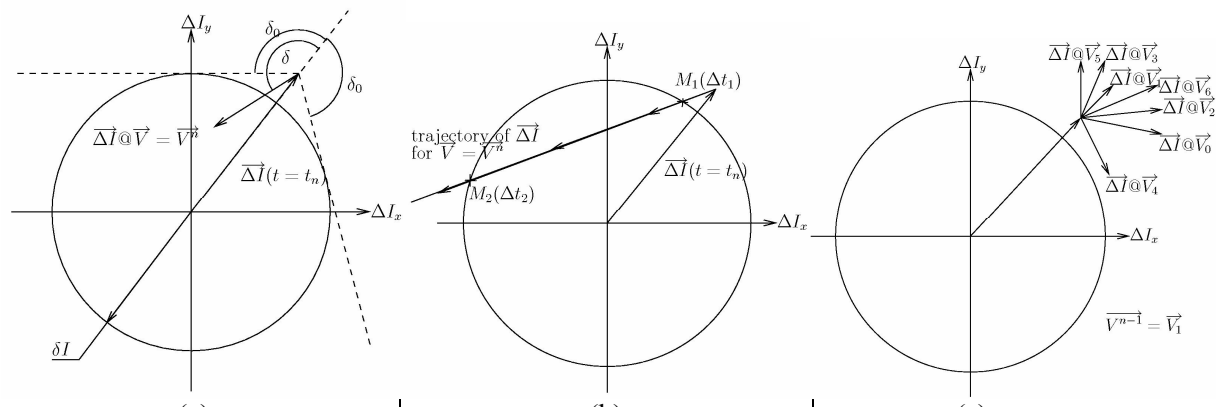

Fig. 9 : (a) Tangency angle δ_0 and incidence angle δ (b) Example of predicted trajectory – Calculation of Δt_2 (c) Divergence of the current vectorial error

If at time t=t_n, the current vectorial error is detected outside of the reference circle, the first step of the predictive controller is to find the optimal vector between those which are *reachable* from the actual vector $\overline{V_{n-1}}$. Whatever the actual vector, there are three vector than can be reach by only one switch on one leg of the inverter. Those are the reachable vectors from $\overline{V_{n-1}}$. On the contrary, the *non-reachable* vectors are the three vectors which are not reachable from $\overline{V_{n-1}}$. A specific attention is given to the two free-wheeling vectors in order not to test both of them. If none of the reachable vectors are able to bring back the current vectorial error in the reference circle, the second step is launched and the non-reachable vectors are tested. If none of the non-reachable vectors are also able to bring back the current vectorial error in the reference circle, the minimization of the quantity $\left|\overline{\Delta I(t_n + \Delta t_{\min})}\right|$ for both reachable and non-reachable vectors from $\overline{V_{n-1}}$ is used to determine the optimal next vector. Moreover, in order to prevent from narrow pulses, a test on the candidate vector at each step is done to respect $\Delta t_{\min}$ on the three legs of the inverter.

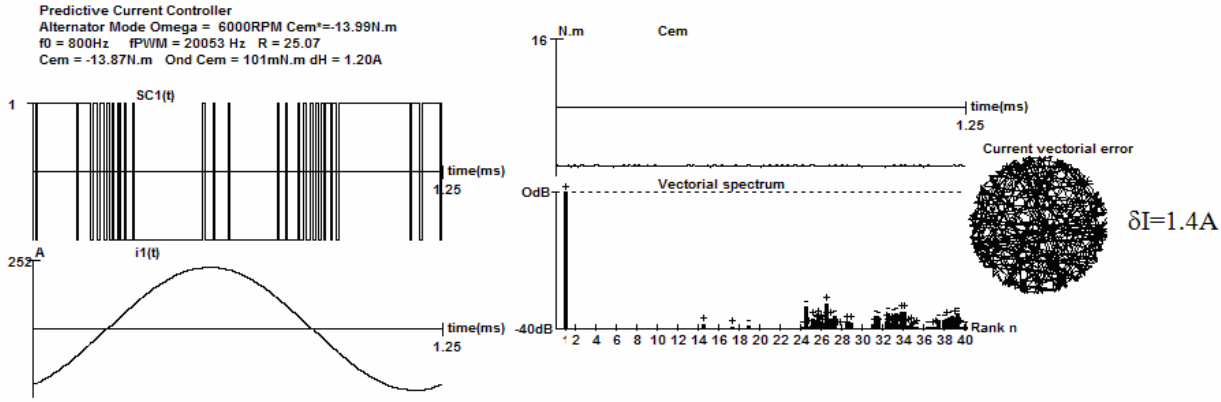

Fig. 10 : Simulation in alternator mode with a predictive current controller

Simulations and Comparisons

For the same operating point of Fig. 5 and Fig. 8, the predictive current controller has performances close to the hysteretic current controller (See Fig. 10). The vectorial spectrum of the strategy has low harmonics at ranks greater than the frequency ratio R. So as to clearly compare these three strategies, simulations were done for different motor speeds and different operating points at a given speed. The operating points

for a given speed differ from each other by the subjacent *modulation index* $m_i = |\overline{V}|/(0.5\times U_{DC})$. For interesting modulation index from 0.5 to $2/\sqrt{3}$ and a given speed, the better machine efficiency operating point is calculated thanks to an optimization program. The parameters Δh and δl will be adapted to maintain a switching frequency close to 20 kHz and each strategies will be evaluated by its *Weighted Total Harmonic Distortion* (WTHD) . The WTHD is defined by:

$$WTHD = \frac{1}{|\overline{V_1}|}\cdot\sqrt{\sum_{n=2}^{\infty}\left(|\overline{V_{n+}}|/n\right)^2 + \left(|\overline{V_{n-}}|/n\right)^2} \qquad (11)$$

A second comparison parameter is the linearity deviation of the strategy when the speed of the SSG increases. In fact, the real modulation index in steady-state m_i differs from the reference modulation index $m_i^* = |\overline{V^*}|/(0.5\times U_{DC})$. Results for two different high speeds are plotted on Fig. 11.

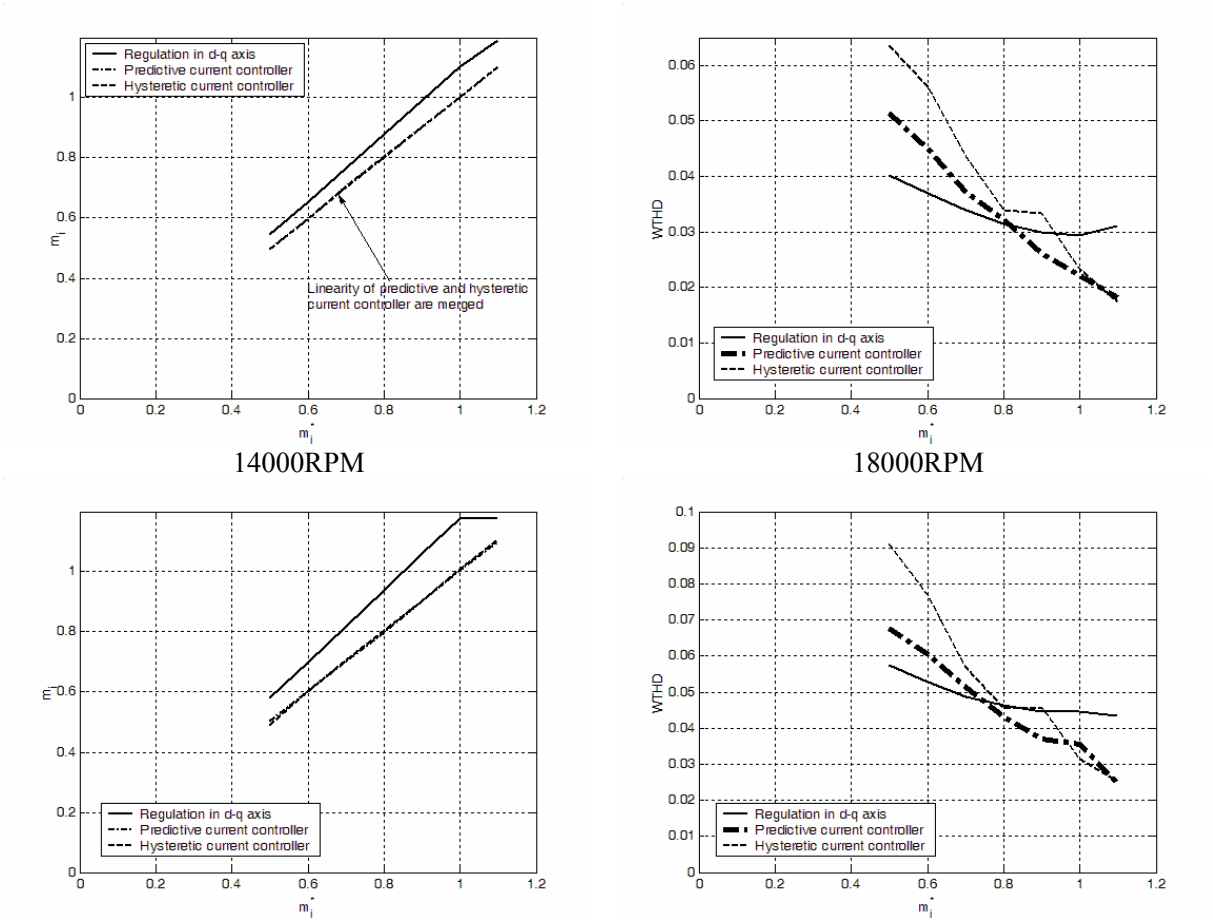

Fig. 11 : Linearity and WTHD at 18000RPM

The linearity's deviation of regulation in d-q axis at high speed is not tolerable. It shows that it is not possible to work in PWM mode at high speed in steady state with SVM technique. On the other hand, hysteretic current controller and predictive current controller keep a satisfactory linearity at high speed. The WTHD of predictive and hysteretic current controller are close at high modulation index (m_i>1) whatever the speed of the SSG. For lower modulation index (0.5 < m_i < 1), the WTHD of the predictive current controller is always better than the hysteretic one. The WTHD of the regulation in d-q axis is not really representative as far as the linearity's deviation is high.

Experimental Implementation

The average execution time of the complete algorithm in simulation on a Pentium M at 1.4GHz is 6µs. As a consequence, the execution time of the embedded algorithm on a 150MHz DSP is 56µs. It is obvious that the average switching frequency of 20KHz is not possible.
However, for a lower switching frequency and in order to compare several PWM techniques, a 10KW powertrain test bench is instrumented. Software dedicated to the PWM strategy will be implemented in a TMS320F2812 evaluation board.
Several measures are envisaged:

- Inverter efficiency thanks to a Yokogawa PZ4000
- Torque quality
- Static and dynamic current error

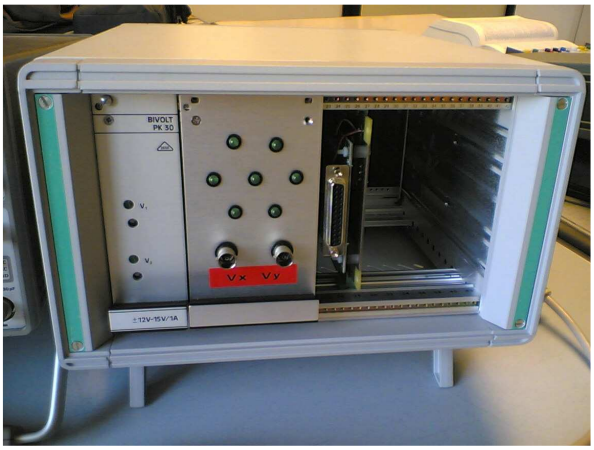

(a)

(b)

Fig. 12 : Experimental test bench (a) Rack dedicated to PWM (b) 10KW powertrain test bench

Conclusion

This paper has shown that the classical regulation in d-q axis is not suitable for a SSG application because of “troubles in the loop” at high speed.
In spite its simplicity, hysteretic current controller is not optimal in theory but has good performances even at high speed (good linearity and low WTHD).
These two reports have led to a design of a predictive current controller. It has better performances than the hysteretic current controller at high speed but requires much more sophisticated electronics (High frequencies FPGA and current sensors).
All tests were done under steady-state operation. Future investigations will highlight dynamic performances of these current controllers.
The spectral characteristics of the predictive current controller allow decreasing the average switching frequency at medium speed as far as the vectorial spectrum is always centered on a rank greater than the frequency ratio R.
Simplicity of the hysteretic current controller and performances close to the predictive one led to the idea of modifying the control of the third leg of the inverter.

Bibliography

[1]. J.M. Miller, Multiple voltage electrical power distribution system for automotive applications, Proc. 31st Intersociety Energy Conversion Engineering Conference (IECEC) - Washington DC - USA, August, 1996.
[2]. C. Plasse, A. Akemakou, P. Armiroli, and D. Sebille, L'alterno-démarreur, du stop&go au groupe motopropulseur mild hybride, Prop'Elec, Aix-en-Provence, March, 2003.
[3]. J. Hobraiche, J.P. Vilain, and M. Chemin, A comparison between PWM strategies in terms of power losses in a three phased inverter - application to a starter generator, EPE PEMC 2004 - Latvia, September, 2004.
[4]. H.W. Van Der Brock, H.Ch Skudelny, and A. Nabae, Analysis and realization of a pulse width modulator based on voltage space vectors, IEEE/IAS Annual Meeting Conference Record, Vol.29, pp412-17, 1988.
[5]. M.P. Kazmierkowski and L. Malesani, Current control techniques for three phases voltage source pwm converters : A survey, IEEE Transactions on Power Electronics, Vol.45, pp.691-703, October, 1998.
[6]. S. Ogasawara, H. Akagi, and G. Stanke. A novel pwm scheme of voltage source inverters based on space vector theory. Archiv für Elektrotechnik, Vol.74, pp 33-41, 1990.
[7]. F. Jenni and D. Wueest. The optimization parameters of space vector modulation. Fifth European Conference on Power Electronics and Applications, IEE - London - UK, 1993.
[8]. J.P. Vilain and C. Lesbroussart. Criteria for the evaluation of three-phase pwm strategies in the case of vectorial approach, EPE PEMC - Budapest - Romania, 1996.
[9]. D.M. Brod and D.W. Novotny, Current control of vsi-pwm inverters, IEEE Transactions on Industry Applications, pp.562-70, 1985.
[10]. J. Holtz. Pulsewidth modulation - a survey. IEEE Transactions on Industrials Electronics, Vol.39, N°5, pp.410-420, December, 1992.
[11]. J.Holtz and S.Statdfeld, A PWM Inverter Drive System with On-line Optimized Pulse Patterns, EPE European Conference on Power Electronics Applications - Brussels - Germany, pp.3.21-3.25, 1985
[12]. J.Holtz and S.Statdfeld, A Predictive Controller for the Stator Current Vector of AC Machines Fed from a Switched Voltage Source, IPEC, Tokyo, pp.1665-75, 1983